24th INTERNATIONAL CONGRESS ON SOUND AND VIBRATION
23–27 July 2017, London

ICSV24
23-27JULY 2017
LONDON CALLING

ACOUSTICAL EDUCTION OF POROUS MEDIA PROPERTIES

Remi Roncen, Frank Simon and Estelle Piot
ONERA, 2 Avenue Edouard Belin, Toulouse, France
email: remi.roncen@onera.fr

The primary goal of this study is to investigate an eduction method aimed at identifying some non-acoustical properties of porous media; its secondary goal is to improve the characterization of the effect of an internal flow on porous media acoustics. Porous materials are increasingly used in exhaust mufflers, acoustic liners and transpiration cooling, with the impact of the flow on their acoustical behavior having received little attention since the pioneering work of Cummings and Chang. The determination of their properties (porosity, permeability, tortuosity,...) is of crucial importance to ensure quality control during the manufacturing process and the knowledge of the laws predicting their physical behavior. The complex pore micro-topology of porous media allows for a valuable sound attenuation in the audible frequencies via phenomena such as viscous friction, thermal exchange and frame vibration. This naturally leads to the development of an acoustical eduction method to retrieve these properties, which are the input parameters of models yielding equivalent propagation characteristics, in the frequency domain. The experimental apparatus consists in a set of two impedance tubes, allowing measurements up to 6000 Hz without flow, and 1500 Hz with flow, where the velocity is kept under 2m/s. The novelty of this study is to undertake the simultaneous eduction of all the parameters of the JCAPL model in the no-flow case and to educe the Biot-Allard parameters in the presence of an internal flow. Eduction results are firstly obtained in synthetic configurations, showing the effectiveness of the present method as an identification tool and its robustness relative to noise. The proposed method is finally applied to a foam sample and an analysis of the mean flow effect is conducted.

Keywords: eduction, porous media, internal flow

1. Introduction

Porous materials are extensively used in a wide range of applications, from geophysics to sound absorption. The precise knowledge of wave propagation inside systems made of porous media is of crucial importance and usually requires the use of finite element models based on the Biot's theory [1]. Additional to the Biot's theory are the semi-phenomenological models used to account for the visco-thermal dissipation of the waves inside the porous medium [2, 3, 4, 5]. The resulting augmented theory, the Biot-Allard model, can be simplified when considering an immobile frame, resulting in an equivalent fluid modeling. A certain number of parameters are needed to adequately represent wave propagation and attenuation in complex porous media: porosity ϕ, tortuosity α_∞, static viscous (resp. thermal) permeability Π_0 (resp. Π_0'), viscous (resp. thermal) characteristic length Λ (resp. Λ'), static viscous (resp. thermal) tortuosity α_0 (resp. α_0'). While direct measurements can be used to access individually some of these parameters, certain drawbacks and difficulties of these methods tend to orient the eduction strategy towards inverse measurements that can possibly yield in a single experiment all the desired parameters, as they all influence the acoustic response of the porous material and can thus be found by the minimization of a proper acoustical cost function, sensitive to all of these parameters.

Another subject of interest lies in the presence of a mean flow inside a porous medium (in exhaust silencers or combustion chamber porous walls) and its impact on the bulk acoustic properties of the material. Following [6], it is expected that an increase in the flow velocity will result in an increase in the material flow resistivity, indicating the appearance of an additional inertial drag.

However, Cummings model rests on a parallel fiber theory that fails to predict all the complex interactions that the Biot-Allard model is capable of predicting in the case of complex pore shapes and non rigid materials. It is expected that some other parameters might be changed by the addition of a flow. Thus, the eduction method can be used to identify the new values, obtained in the presence of a flow in order to yield more accurate prediction capabilities in these configurations.

To investigate the aforementioned issues, the present article is organized as follow: Section 2 details the equivalent fluid model and the two experimental devices; the eduction method follows in Section 3; the impact of an internal mean flow is studied in Section 4 and the properties are yet again educed with the tools described in the previous Sections. Concluding remarks are laid out in Section 5.

2. Acoustics of porous materials

2.1 The equivalent fluid model

In the simplified case where the porous solid phase is assumed rigid, only airborne waves propagate in the material. The contribution of the solid phase to the acoustics is negligible and one can see the porous medium as an equivalent fluid subject to visco-thermal losses due to the high surface contact ratio between the fluid and solid phases and to the complex shape of the pores. Following [7] and assuming total decoupling between visco-inertial and thermal effects, one obtains the complex-valued Helmholtz equation:

$$\Delta p + \omega^2 \frac{\tilde{\rho}_{\text{eq}}}{\tilde{K}_{\text{eq}}} p = 0 \tag{1}$$

where a tilde indicates a complex frequency-dependent property, p is the interstitial pore pressure, ω is the pulsation, $\tilde{\rho}_{\text{eq}}$ is the equivalent density of the fluid disregarding thermal effects and $\tilde{K}_{\text{eq}}$ is the equivalent bulk modulus of the fluid disregarding viscous effects. Semi-phenomenological models for $\tilde{\rho}_{\text{eq}}$ and $\tilde{K}_{\text{eq}}$ can be obtained for different simplified pore geometries by using the limits of low or high frequency regimes, where the fluid is fully viscous-isothermal or potential-adiabatic, respectively. Using the model of Johnson, Champoux, Allard, Pride and Lafarge (JCAPL) [2, 3, 4, 5], one has $\tilde{\rho}_{\text{eq}} = \tilde{\rho}_{\text{eq}}\left(\phi, \alpha_\infty, \Pi_0, \Lambda, \alpha_0\right)$ and $\tilde{K}_{\text{eq}} = \tilde{K}_{\text{eq}}\left(\phi, \Lambda', \Pi_0', \alpha_0'\right)$ (see [8, p. 83-84] for full expressions). Some insight into the model parameters are now given: ϕ is the material porosity and represents the volume fraction of air in the material, ranging from 0 to 1 and typically very close to 1 for foams used in acoustic insulation; α_∞ is the tortuosity, a value larger than 1 representing the apparent increase in the equivalent fluid density due to the dispersion of the microscopic velocity inside complex pores, in the high frequency limit; Π_0 is the static viscous permeability (unit m^2), an intrinsic material property related to the flow resistivity σ_0 by the relation $\Pi_0 = \mu/\sigma_0$, where μ is the fluid dynamic viscosity; Λ is the viscous length (unit m), it was introduced in [2] and represents an equivalent hydraulic radius of the smaller pores, where viscous effects dominate; Λ' is the thermal length (unit m), it was introduced in [3] and represents the equivalent hydraulic radius of the larger pores, where thermal effects dominate; Π_0' is the static thermal permeability (unit m^2), introduced in [9] as the thermal counterpart of Π_0 and links the excess temperature in a pore to the pressure variation; α_0 is the static viscous tortuosity, an inertial factor introduced in a different form by [4] and corrected by [5], it represents the apparent increase in the equivalent fluid density due to the form drag in the low frequency limit when the pores have constrictions ; α_0' is the static thermal tortuosity, introduced as a shape factor by [4] and further corrected in [5] to adjust the bulk modulus values in the low frequency range when the material pores have constrictions. The aforementioned notion of low and high frequency is material dependent and differs for viscous (f_ν) and thermal (f_τ) effects as follow:

$$f_\nu = \frac{\phi\nu}{2\pi\Pi_0\alpha_\infty}, \quad f_\tau = \frac{\nu'}{2\pi\Lambda'^2}, \tag{2}$$

with ν the air cinematic viscosity and $\nu' = \nu/\,\mathrm{Pr}$, Pr being the Prandtl number.

To efficiently model the wave propagation inside a porous material, one has to know the above-mentioned parameters and their impact on the acoustic response of the material. The eduction method consists in using the latter to infer the former. We proceed by first describing the experimental devices used in this work to acquire the information used to educe the parameters in Section 3.

2.2 Impedance and transmission tubes

Two experimental devices are used in this study, as shown in Fig. 1. The first one is an impedance tube, used to measure the reflection coefficient of a material placed above a rigid backing (for which the reflection coefficient is known), thus obtaining the surface impedance of the material as defined by $Z_s = p/v$ with p (resp. v) the pressure (resp. the normal velocity) just in front of the material. The experimental apparatus consists of a $38\,\mathrm{mm}$ diameter tube, equipped with two microphones (whose in-between distance can be adjusted), allowing the measurement of the surface impedance in the $200 - 6000\,\mathrm{Hz}$ range (plane wave hypothesis).

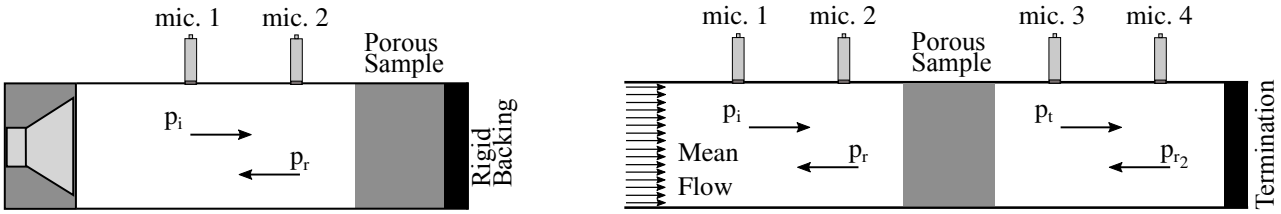

Figure 1: Impedance tube (left) and transmission tube (right) experimental set up

The second experimental device consists of a transmission tube of square cross-section where it is possible to generate a flow up to approximately $2\,\mathrm{m/s}$ passing through a porous material, superimposed with acoustic waves. The pressure measurements at four locations yield the Transfer Matrix [10] linking the pressure and velocity on both sides of the material, up to a frequency of $1500\,\mathrm{Hz}$ (plane wave hypothesis). The Transfer Matrix $\boldsymbol{T}$ can be measured with only four microphones and one termination condition in the case of an isotropic material, yielding:

$$\boldsymbol{T} = \begin{pmatrix} T_{11} & T_{12} \\ T_{21} & T_{22} \end{pmatrix} = \begin{pmatrix} \cos\left(\tilde{k}_{\mathrm{eq}} d\right) & j\tilde{z}_{\mathrm{eq}} \sin\left(\tilde{k}_{\mathrm{eq}} d\right) \\ j\tilde{z}_{\mathrm{eq}}^{-1} \sin\left(\tilde{k}_{\mathrm{eq}} d\right) & \cos\left(\tilde{k}_{\mathrm{eq}} d\right) \end{pmatrix}, \tag{3}$$

where $\tilde{k}_{\mathrm{eq}} = \omega/\tilde{c}_{eq}$ is the equivalent wave number, $\tilde{c}_{eq} = \sqrt{\tilde{K}_{\mathrm{eq}}/\tilde{\rho}_{\mathrm{eq}}}$ is the equivalent speed of sound and $\tilde{z}_{\mathrm{eq}} = \tilde{\rho}_{\mathrm{eq}}\tilde{c}_{eq}$ is the characteristic impedance of the material. If we now suppose the material to be rigidly-backed, we can obtain the dimensionless surface impedance ($-j\omega t$ convention, [8, p. 19]):

$$Z_s = -j\tilde{z}_{\mathrm{eq}} \cot\left(\tilde{k}_{\mathrm{eq}} d\right) / Z_0, \tag{4}$$

with d the width of the material and $Z_0 \approx 420\,\mathrm{kg.m^{-2}.s}$ the impedance in free air. One can note that this surface impedance is directly retrieved with: $Z_s = T_{11}/T_{21}/Z_0$, so this is the only quantity we will be discussing hereafter.

3. Eduction method

3.1 Principle of the method

The eduction method has for sole purpose the inference of a set of parameters describing the homogenized properties of the materials from a finite number of measured acoustic signals related to the material, such as its surface impedance. The global methodology is now described.

- The surface impedance of a sample can be measured in a certain frequency range, with either of the apparatuses described in Section 2.2. Different experiments, performed on the same material, could be used to increase the available information provided by the data space, for instance by putting an air gap behind the material [11], by using different sample widths or by performing some prior direct measurements of readily accessible material properties, such as its porosity. A cost function $\mathcal{J}$ is then defined as the discrete sum on the frequencies under scrutiny ω_i of the squared distance between the q measured signals and the ones stemming from the modeling, taking as input the parameter vector $\boldsymbol{\theta} = (\phi, \alpha_\infty, \Pi_0, \Lambda, \alpha_0, \Lambda', \Pi_0', \alpha_0')^t$ to be inferred. We can write the dimensionless cost function as:

$$\mathcal{J}(\boldsymbol{\theta}) = \sum_q \sum_{\omega_i} \left| Z_{s,\,\text{meas}}(\omega_i) - Z_{s,\,\text{model}}(\omega_i, \boldsymbol{\theta}) \right|^2 / \sum_q \sum_{\omega_i} \left| Z_{s,\,\text{meas}}(\omega_i) \right|^2 . \tag{5}$$

- The cost function $\mathcal{J}$ is then minimized with respect to $\boldsymbol{\theta}$ using a Differential Evolution algorithm [12], a stochastic direct search method well-suited to non-linear multi-modal cost functions and global minimization tasks. It consists in the generation of populations of points in the model space, that are evolved through mutation and crossover operations. The best candidates are then selected with a greedy criterion in order to yield better-suited populations, until convergence is obtained. No initial guess is needed, as the first population is randomly generated in order to cover the model space, which renders the algorithm quite useful when no prior knowledge of the material is available.
- To evaluate the relative precision of the obtained parameters, a local sensitivity analysis is performed around the minimum of the cost function.

3.2 Eduction results

3.2.1 Synthetic case

First, the eduction process is applied to the simulated synthetic data of a material inside an impedance tube for frequencies in the range $200 - 6000\,\text{Hz}$, representative of the black foam that is experimentally tested in Section. 3.2.2. A set of parameters $\boldsymbol{\theta}_{i,0}$ is chosen with values taken as the ones directly measured for the black foam under study (except for α_0 and α_0', which are taken at random), and the JCAPL model is used to calculate the corresponding surface impedance $Z_{s,0}$, for a $35.9\,\text{mm}$ width material. A white noise is then added to the impedance to take into account errors in both the measurements and the modeling (observational and modeling uncertainties are combined by addition of their covariance operators when using a Gaussian assumption [13, p. 35-36], which justifies the encompassing of both errors into the same white noise). The noise amplitude is set to ϵZ_0, where ϵ is the noise ratio. The educed parameters $\check{\theta}_i$ are shown in Table 1 for two noise levels ($\epsilon = 0.2$ and $\epsilon = 0.5$).

Despite the high noise added to the synthetic measurements, the eduction provides most of the parameters with a good accuracy. Exception is made for the thermal parameters Λ', Π_0' and α_0' at the highest noise level. For the considered foam, we obtain with Eq. (2) $f_\nu \approx 357\,\text{Hz}$ and $f_\tau \approx 301\,\text{Hz}$, which might explain why the eduction fails to correctly identify these parameters when the noise ratio is high: the lower limit of $200\,\text{Hz}$ we imposed on the frequency range is too high to allow the present

Table 1: Synthetic configuration eduction results

θ_i	ϕ	α_∞	σ_0	Λ	Λ'	Π'_0	α_0	α'_0
Units	/	/	$\mathrm{N.s.m^{-4}}$	μm	μm	$.10^{-10}\,\mathrm{m^2}$	/	/
$\theta_{i,0}$	0.96	1.14	3100	230	307	142	1.5	1.3
$\check{\theta}_i$, ϵ= 0.2	0.96	1.13	3170	213	321	139	1.47	1.28
$\check{\theta}_i$, ϵ= 0.5	0.98	1.11	3260	164	537	242	1.46	1.73

cost function to "see" much influence of Λ', Π'_0 and α'_0. However, it is interesting to note that for lower noise ratios, these parameters seem well-estimated despite having no access to measurements at very low frequencies.

3.2.2 Black foam

The eduction method is now applied to the experimental results obtained with the black foam (namely, its surface impedance). Results are shown in Table 2 and in Fig. 2. We can see the excellent match between the educed parameters and the measurements, while there is a significant difference with $Z_{s,0}$, the impedance calculated using the directly measured parameters. It is shown that the present method of identification yields a set of parameters that allow a better representation of the acoustic behavior of the material. Most of the disagreement between these two curves is shown to be driven by the viscous length parameter Λ, which varies from the directly measured value by around 30%.

Table 2: Black foam eduction results (same units as in Table 1)

θ_i	ϕ	α_∞	σ_0	Λ	Λ'	Π'_0	α_0	α'_0
$\theta_{i,0}$	0.96	1.14	3100	230	307	142	N/A	N/A
$\check{\theta}_i$	0.958	1.166	2897	155	298	129	1.46	1.43
Mismatch	0.2%	2.3%	6.5%	32.6%	2.9%	9.2%	N/A	N/A
Bounds	0.95-0.97	1.16-1.17	2840-3000	152-158	281-355	108-136	1.46-1.48	1.36-1.55

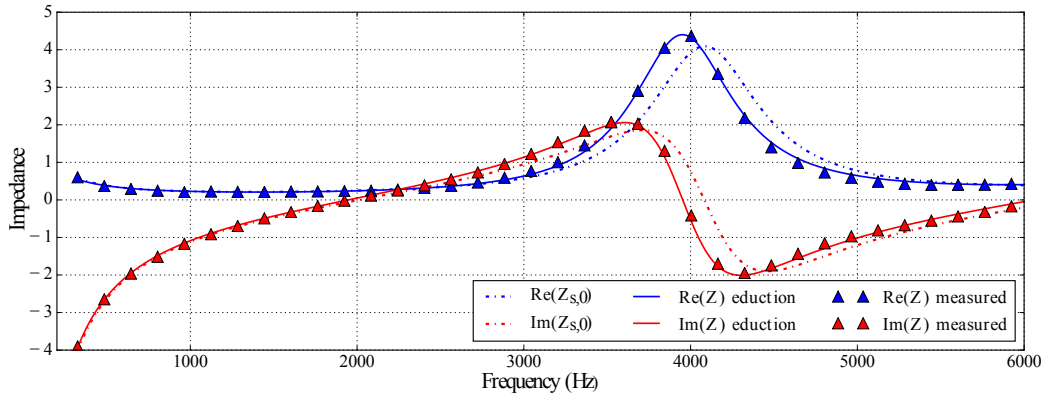

Figure 2: Black foam impedance fit

A local sensitivity analysis is then performed by varying the parameters around their educed value. By setting a limit at 0.1% of the dimensionless cost function, we can give lower and upper bounds for the parameters, as summarized in the last line of Table 2. The narrower the bounds, the more sensitive the parameter. The most influential parameters, relatively to the cost function, are ϕ, α_∞, σ_0, Λ and α_0. It is notable that in this case, the cost function appears very sensitive to α_0, whereas this parameter is often neglected in the literature (mostly because it is hard to measure). A global sensitivity analysis

[14] should be performed to investigate with further details the phenomenon, which is most likely related to the low value of the flow resistivity, indicating that form drag could be dominant in a larger frequency range.

4. Influence of an internal mean flow on poroelastic media acoustics

4.1 Preamble

The goal of this section is to describe the influence of an internal flow on porous media acoustics. Following [6], it is expected that the flow resistivity be increased by an inertial factor σ_i, as:

$$\sigma_{\text{tot}} = \sigma_0 + \sigma_i \left| v \right| , \tag{6}$$

where v is the bulk velocity. The novelty of this study is to inquire the validity of this assumption in the more general context of the Biot-JCAPL model (the Biot-Allard model in which the extensions of Pride and Lafarge are taken into account), by means of an eduction method applied to dedicated experimental results.

4.2 Experimental setup

A square section transmission tube is adapted as depicted in Fig. 1 to superimpose a bulk flow of maximum velocity $2\,\mathrm{m/s}$ with acoustic waves, generated in the frequency range $200-1500\,\mathrm{Hz}$. A $10\,\mathrm{cm}$ large melamine foam is placed in the test section, its transfer matrix is measured for different flow speeds and the corresponding surface impedance is extracted with Eq. (4). The material, clamped to avoid being ejected while subjected to a mean internal flow, displays a different behavior from that of an equivalent fluid, namely, the presence of a peak in the real part of the impedance, when the reactance is zero. This peak is usually explained by the existence of a $\lambda/4$ resonance of the frame-borne wave [8, Chap. 6] and is related to the material stiffness and density. To palliate the modeling shortcomings, the full Biot-Allard model is used in this section. As it is not in the scope of this study to detail such a model and educe the 3 supplementary elastic properties of the material (namely, the shear modulus N, the damping factor η_s and the Poisson ratio ν_s), we will not delve into the full detail of the implementation; it suffices to know that the shear modulus and the Poisson ratio characterize the stiffness of the frame, while the damping factor allows the shear modulus to take complex values to account for elastic dissipation: $\tilde{N} \leftarrow N(1 + j\nu_s)$. The same eduction strategy as in Section 3 is followed. Due to the low frequency range considered in this study, it is not expected that high frequency parameters be too influential and it is thus not expected that the eduction provides accurate results for them. As our focus is on the low frequency range, this is not too detrimental. Hereafter, we fix a certain number of parameters, as given by the eduction when there is no internal flow: $\phi = 0.97$, $\alpha_\infty = 1.4$, $\sigma_0 = 16400\,\mathrm{N.s.m^{-4}}$, $\Lambda = 39\,\mu\mathrm{m}$, $\Lambda' = 70\,\mu\mathrm{m}$, $\Pi'_0 = 11.10^{-10}\,\mathrm{m^2}$, $\alpha_0 = 1.53$ and $\alpha'_0 = 2$. The only parameters that were allowed to vary between the three eduction processes were the flow resistivity σ_{tot} and the elastic parameters (N, η_s and ν_s). Direct measurements were conducted by means of static pressure probes to access the foam flow resistivity at different bulk velocities ranging from 0 to $2\,\mathrm{m/s}$, yielding $\sigma_0 \approx 17700\,\mathrm{N.s.m^{-4}}$ and $\sigma_i \approx 2600\,\mathrm{N.s^2.m^{-5}}$. It should be noted that the goal of this section is not the precise identification of the parameters, but the study of their evolution in the presence of an internal mean flow.

4.3 Eduction with flow

Experimental measurements of the impedance, along with the impedance calculated with the educed parameters are shown in Fig. 3. Three mean flow values were tested, by varying the mass flow. It can be observed that the tendency for both the real and imaginary parts of the surface impedance

are well-reproduced by the impedance model, which proves the effectiveness of the eduction method. In Table 3, the eduction results are displayed, along with the direct measurement performed for σ_i.

θ_i	$\sigma_i(\mathrm{N.s^2.m^{-5}})$	N (Pa)	η_s	ν_s	K_c(Pa)
Direct measure	2600 ± 100	N/A	N/A	N/A	N/A
$\check{\theta}_i$, $v = 0\,\mathrm{m/s}$	N/A	$5.64.10^5$	0.132	0.012	$1.14.10^6$
$\check{\theta}_i$, $v = 0.93\,\mathrm{m/s}$	2883	$5.41.10^5$	0.143	0.014	$1.1.10^6$
$\check{\theta}_i$, $v = 1.62\,\mathrm{m/s}$	2975	$5.41.10^5$	0.138	0.009	$1.09.10^6$

Table 3: Eduction results for the foam with internal mean flow

A satisfactory accordance can be found between the educed σ_i and the measured one, showing the effectiveness of the method in the identification of this parameter. When the flow is increased, the inertial factor σ_i is almost constant, which proves the validity of the linear law Eq. (6). Another interesting phenomenon is the shifting of the impedance peak towards lower frequencies along with its narrowing, when the bulk flow velocity is increased, as seen in Fig. 3 in the $600-800\,\mathrm{Hz}$ range. The parameter most related to this behavior is believed to be the elasticity coefficient of the frame in vacuum $K_c = 2N(1-\nu_s)/(1-2\nu_s)$. It is apparent than an increase in the internal mean flow velocity tends to reduce K_c (even if it becomes less marked as the velocity increases), resulting in the displacement of the impedance peak. The sensitivity of η_s was found to be low in this case, and no clear conclusion could be drawn regarding its value. Further studies should be conducted to investigate this phenomenon with more details, as only one foam sample was available for this experiment.

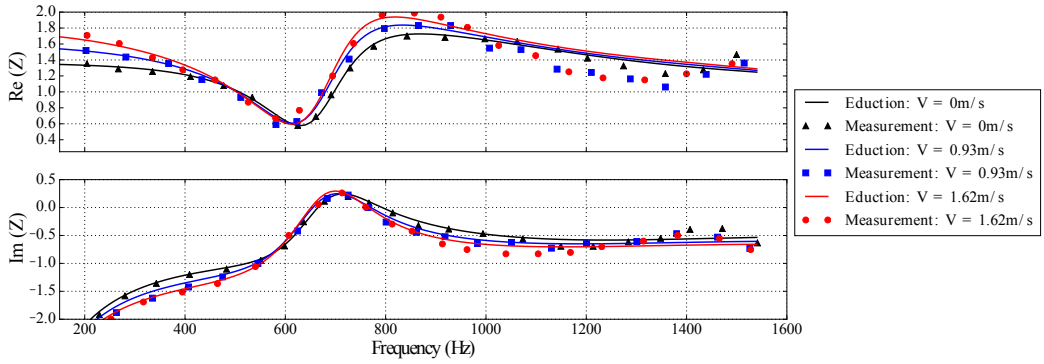

Figure 3: Surface impedance of a melamine foam with internal mean flow variation

5. Conclusion

The present study has discussed an eduction method aimed at identifying porous media properties represented by either an equivalent fluid (JCAPL model) or the full Biot-Allard model, showing the robustness of such a method. The eduction was first conducted on a synthetic case, before it was tried on a real experiment for a highly porous foam with low resistivity, where the impedance appeared very sensitive to the low frequency limits of the viscous dynamic tortuosity, α_0. The impact of an internal mean flow on porous media acoustics was investigated with a melamine foam sample, for two different flow velocities. As the foam was structurally constrained, a behavior different than that of an equivalent fluid model was observed, and the Biot-Allard model was used to educe the properties of the material in the presence of an internal mean flow. The increase in the flow velocity was shown to have two main impacts: the flow resistivity of the material was increased, following Cummings theory, and the elasticity coefficient of the frame was decreased, shifting the impedance peak towards lower frequencies and narrowing it. These results show that for such a poroelastic material, even low

velocities are sufficient to induce a different acoustic behavior. These results should be confirmed for a larger panel of flow resistivity.

Acknowledgment

This research has been financially supported by the French region Occitanie and ONERA (the French Aerospace Lab). The authors are grateful to Fabien Chevillotte (MATELYS) for providing the black foam experimental data.

References

1. Biot, M. A. Mechanics of deformation and acoustic propagation in porous media, *Journal of applied physics*, **33** (4), 1482–1498, (1962).

2. Johnson, D. L., Koplik, J. and Dashen, R. Theory of dynamic permeability and tortuosity in fluid-saturated porous media, *Journal of fluid mechanics*, **176**, 379–402, (1987).

3. Champoux, Y. and Allard, J.-F. Dynamic tortuosity and bulk modulus in air-saturated porous media, *Journal of applied physics*, **70** (4), 1975–1979, (1991).

4. Pride, S. R., Morgan, F. D. and Gangi, A. F. Drag forces of porous-medium acoustics, *Physical review B*, **47** (9), 4964, (1993).

5. Lafarge, D., *Propagation du son dans les matériaux poreux à structure rigide saturés par un fluide viscothermique: Définition de paramètres géométriques, analogie electromagnétique, temps de relaxation*, Ph.D. thesis, (1993).

6. Cummings, A. and Chang, I. Acoustic propagation in porous media with internal mean flow, *Journal of sound and vibration*, **114** (3), 565–581, (1987).

7. Zwikker, C. and Kosten, C. W., *Sound absorbing materials*, Elsevier (1949).

8. Allard, J.-F. and Daigle, G. Propagation of sound in porous media: Modeling sound absorbing materials, *The Journal of the Acoustical Society of America*, **95** (5), 2785–2785, (1994).

9. Lafarge, D., Lemarinier, P., Allard, J. F. and Tarnow, V. Dynamic compressibility of air in porous structures at audible frequencies, *The Journal of the Acoustical Society of America*, **102** (4), 1995–2006, (1997).

10. Song, B. H. and Bolton, J. S. A transfer-matrix approach for estimating the characteristic impedance and wave numbers of limp and rigid porous materials, *The Journal of the Acoustical Society of America*, **107** (3), 1131–1152, (2000).

11. Zieliński, T. G. Normalized inverse characterization of sound absorbing rigid porous media, *The Journal of the Acoustical Society of America*, **137** (6), 3232–3243, (2015).

12. Storn, R. and Price, K. Differential evolution–a simple and efficient heuristic for global optimization over continuous spaces, *Journal of global optimization*, **11** (4), 341–359, (1997).

13. Tarantola, A., *Inverse problem theory and methods for model parameter estimation*, SIAM (2005).

14. Ouisse, M., Ichchou, M., Chedly, S. and Collet, M. On the sensitivity analysis of porous material models, *Journal of Sound and Vibration*, **331** (24), 5292–5308, (2012).